COBEM 2023 27TH INTERNATIONAL CONGRESS OF MECHANICAL ENGENEERING

ABCM Brazilian Society of Mechanical Sciences and Engineering
27th ABCM International Congress of Mechanical Engineering
December 04-08, 2023, Florianópolis-SC, Brazil

COB-2023-0031
ARTIFICIAL IMMUNE SYSTEM APPLIED IN THE DETECTION OF DAMAGE IN AN INVERTED PENDULUM UNDER THE EFFECT OF A CONTROLLER

Matheus Medeiros Donatoni
Faculdade de Engenharia de Ilha Solteira, UNESP - Universidade Estadual Paulista, Department of Mechanical Engineering,
Ave. Brasil, 56, 15385-000 – Ilha Solteira, SP, Brazil
matheus.m.donatoni@unesp.br

Fabio Roberto Chavarette
Instituto de Química - Câmpus de Araraquara, UNESP - Universidade Estadual Paulista, Department of Engineering, Physics and Mathematics,
St. Prof. Francisco Degni, 55, 14800-060 - Araraquara, SP, Brazil
fabio.chavarette@unesp.br

Abstract. *Control systems are experienced in everyday life and provide optimization for several tools and systems that human beings rely on. In some cases, the usage of controllers in dynamic systems directly aims at their applicability and safety increment, hence their proper functioning is directly linked to the appropriate target plant modeling. Considering these points and the different possibilities of damage that dynamic systems can suffer due to the nature of their operation, the need for monitoring the structural health of these systems, which may have their physical characteristics modified, is validated. A commonly used technique for this purpose is Structural Health Monitoring (SHM), which is a data-driven system that can help detect failures, therefore allowing appropriate action arising from an early prognosis. Since it's based on the detection of patterns, a suitable tool used for this purpose is the so-called Artificial Immune System (AIS) which, compared to the Natural Immune System (NIS), is based on the differentiation between self and non-self agents for the classification of signals. In this paper, we propose the application of a SHM system, with AIS as a pattern recognition tool applied to a Rotary Inverted Pendulum (RIP) as a reference model for damage detection in controlled dynamic systems. Since this mechanical system is naturally unstable, its operation is directly dependent on the existence of a controller, which must be able to guarantee its stability and the desired dynamic behavior, such as variable reference tracking. The approach taken uses the some of the controller state variables as the data for monitoring and classifying operational conditions. The proposed technique applied to the analysis of four different structural state conditions, with the combination of multiple sensor data, came in a damage detection rate of 99.07%, and a full classification capability.*

Keywords: *Structural health monitoring, Artificial immune systems, Controlled systems, Damage detection, Dynamic mechanical systems.*

1. INTRODUCTION

Control theory consists in the implementation of autonomous dynamic systems (Dorf and Bishop, 2017). Since the 1930s, advancements in frequency response methods have facilitated the practical design of controllers that meet desired specifications. Alongside advancements in computational capabilities, control systems have gained widespread usage in both industrial and everyday applications (Franklin *et al.*, 2010). To ensure effective response within a broad range of operating states, control systems rely on a consistent model that accurately represents their dynamics, enabling the implementation of optimal control laws (Ogata, 2010).

This paper focuses on the Rotary Inverted Pendulum (RIP) as a benchmark model for detecting damage in controlled dynamic systems. Within this context, damage refers to any type of anomaly that can impact the overall performance of the system. According to Frank (1990), three types of damage can occur in dynamic systems: component damage (CD), which involves the failure of a mechanical part within the system; actuator damage (AD), which occurs due to the failure of the actuator assembly in a mechanical system, such as motors; and instrument damage (ID), which arises when monitoring sensors fail to collect data. The presence of damage is expected to alter properties such as stiffness, mass, or energy dissipation modes (Sohn, 2007). Consequently, monitoring the health of the system can proactively anticipate the occurrence of undesired behaviors that may compromise productivity, functionality, and even safety (Isermann, 2006).

Structural Health Monitoring (SHM) encompasses a well-defined set of processes aimed at implementing a damage identification strategy in engineering infrastructures. The strategy can be summarized in four steps: operational evaluation, data acquisition, feature extraction, and statistical modeling for feature classification. In essence, data series are obtained

during different operating conditions of a system and must be processed by mathematical tools capable of indicating their patterns. Once the healthy condition (baseline) is known, a statistical analysis is performed to determine which data differ from it, being classified as damage. (Farrar and Worden, 2007; Figueiredo *et al.*, 2009; Tokognon *et al.*, 2017)

The mathematical tool employed in this paper for data processing is a specific type of algorithm known as an Artificial Immune System (AIS). AIS refers to a collection of algorithms that emulate the operational principles of the Natural Immune System (NIS), primarily employed for pattern recognition, classification, and data clustering. Within the AIS framework, algorithms are classified based on the replication of NIS concepts. The algorithm implemented in this study is based on the Negative Selection (NS) mechanism observed in the classical view of NIS, which enables the discrimination between self and non-self agents. (Engelbrecht, 2007; Talbi, 2009; Almeida, 2022)

In certain instances, traditional methods for damage detection in dynamic systems, such as ultrasonic inspection, X-rays, and acoustic emission testing, may not be feasible. In such cases, modal and/or temporal analyses are employed as alternative approaches, which are well-established methods. However, these analyses entail significant additional costs due to the requirement for specialized equipment, software utilization, and the involvement of expert professionals. Consequently, there is a motivation for Structural Health Monitoring (SHM) methods to generate analysis outcomes based on alternative techniques. (Farrar and Worden, 2012; Almeida *et al.*, 2022)

This article presents the implementation of intelligent damage monitoring in closed-loop control structures, utilizing existing controller data for analysis. By utilizing angular displacements collected for control purposes, the opportunity for damage monitoring arises without the need for additional hardware complexity. Under various operating conditions, including healthy and simulated CD and AD, data is collected while the pendulum remains in its vertical position and its rotary arm follows a square wave pattern. The collected data is then used to train the AIS algorithm to recognize proper signals and determine the presence of damage. Additionally, a second scenario is created to test and categorize random signals based on their similarity to the existing database of known operating conditions.

The remainder of this study is organized as follows. Section 2 presents the mathematical modeling of the physical system and develops the controller used. Section 3 provides the complete development of the SHM system, with details of the experimental execution, AIS algorithm and results discussion. Finally, Section 4 presents the main conclusions of this paper.

2. ROTARY INVERTED PENDULUM MODELING AND CONTROL

The RIP is an electromechanical system composed of a pendulum, a rotary arm, an electric motor and two incremental encoders for angular displacement data acquisition. Only the rotary arm is actuated and it moves in order to keep the pendulum in its upward vertical position. Due to its underactuated nature, inherent instability, and nonlinear dynamics, the RIP requires the implementation of a controller to ensure its proper functioning. (Yang *et al.*, 2009)

Figure 1 shows the schematic representation of the system, with indications of variables and their directions and senses. The variables θ and α are positive in the counterclockwise (CCW) direction and represent the angle between the rotary arm and the x_0 axis and the angle between the pendulum and an axis parallel to z_0 that follows the point M, respectively. The L_r represents the arm length, J_r its moment of inertia, L_p represents the pendulum length, m_p its mass and J_p its moment of inertia in respect to its gravity center. The origin is represented by O, M represents the point where the pendulum shaft bearing is and GC is the pendulum gravity center.

The differential equations that govern the system's motion are obtained through the Euler–Lagrange equations as demonstrated by Rao (2009). They are represented by:

$$\begin{aligned}
\tau_m - B_r\dot{\theta} &= \left(m_pL_r^2 + \frac{1}{4}m_pL_p^2 - \frac{1}{4}m_pL_p^2\cos\alpha^2 + J_r\right)\ddot{\theta} - \left(\frac{1}{2}m_pL_pL_r\cos\alpha\right)\ddot{\alpha} \\
&\quad + \left(\frac{1}{2}m_pL_p^2\sin\alpha\cos\alpha\right)\dot{\theta}\dot{\alpha} + \left(\frac{1}{2}m_pL_pL_r\sin\alpha\right)\dot{\alpha}^2 \\
-B_p\dot{\alpha} &= -\left(\frac{1}{2}m_pL_pL_r\cos\alpha\right)\ddot{\theta} + \left(J_p + \frac{1}{4}m_pL_p^2\right)\ddot{\alpha} - \left(\frac{1}{4}m_pL_p^2\cos\alpha\sin\alpha\right)\dot{\theta}^2 \\
&\quad - \frac{1}{2}m_pL_pg\sin\alpha
\end{aligned} \tag{1}$$

Where $\dot{\theta}$, $\ddot{\theta}$ are rotary arm angular velocity and angular acceleration, respectively. The terms $\dot{\alpha}$, $\ddot{\alpha}$ are pendulum angular velocity and angular acceleration, respectively. The terms τ_m, B_r and B_p come from non-conservative effects and refer to the torque applied to the rotary arm by the motor, the damping terms of the bearing shafts of the rotary arm and pendulum, respectively. And g is the gravity constant.

The system model is used for the development of a Full State Feedback (FSF) controller. This system can be represented in state-space form when linearized, according to Machado (2007) for equilibrium points such as the upward position, which is the case of this application, linearization can be done by applying Taylor series up to the first order to

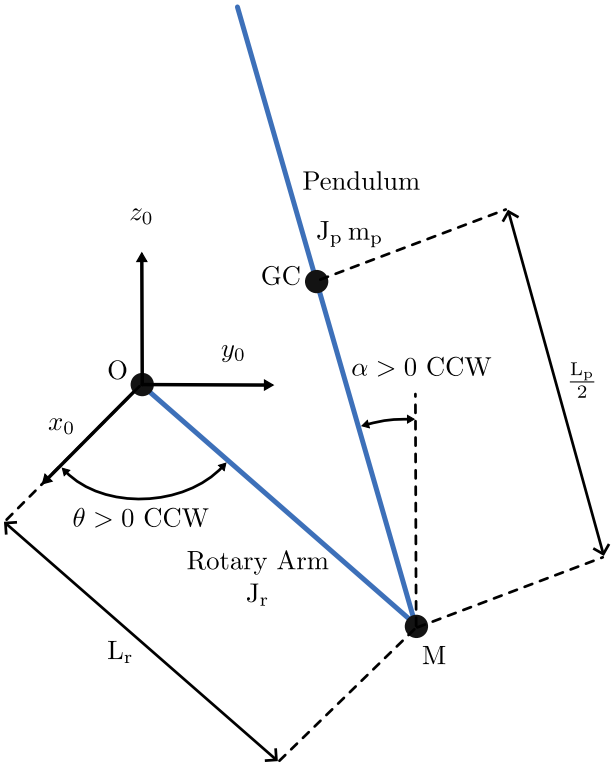

Figure 1: RIP schematic representation and variable conventions.

the Eq. (1), considering all the initial terms null, it can be rewritten in its linear form as:

$$\begin{aligned} \tau_m - B_r\dot{\theta} &= \left(-\frac{1}{2}m_p L_p L_r\right)\ddot{\alpha} + \left(m_p {L_r}^2 + J_r\right)\ddot{\theta} \\ -B_p\dot{\alpha} &= \left(\frac{1}{4}m_p L_p^2 + J_p\right)\ddot{\alpha} - \left(\frac{1}{2}L_p L_r m_p\right)\ddot{\theta} - \frac{1}{2}m_p L_p g\alpha \end{aligned} \tag{2}$$

In the control process, the torque τ_m, present in the Eq. (2), is modified by varying the voltage applied to the motor. It can be replaced by:

$$\tau_m = A_m V_m - B_m\dot{\theta} \tag{3}$$

Where V_m represents the voltage applied to the motor, A_m and B_m represent the motor constant gain and the motor damping due to dissipative effects, respectively. Its state, represented by $\mathbf{x}$, is defined as:

$$\mathbf{x}^{\mathrm{T}} = \begin{bmatrix} x_1 & x_2 & x_3 & x_4 \end{bmatrix} = \begin{bmatrix} \theta & \alpha & \dot{\theta} & \dot{\alpha} \end{bmatrix} \tag{4}$$

Where x_1, x_2, x_3 e x_4 are alias terms for θ, α, $\dot{\theta}$ and $\dot{\alpha}$, respectively. Its derivative, represented by $\dot{\mathbf{x}}$, is given by:

$$\dot{\mathbf{x}}^{\mathrm{T}} = \begin{bmatrix} x_3 & x_4 & \dot{x}_3 & \dot{x}_4 \end{bmatrix} = \begin{bmatrix} \dot{\theta} & \dot{\alpha} & \ddot{\theta} & \ddot{\alpha} \end{bmatrix} \tag{5}$$

Where $\dot{x}_3$ e $\dot{x}_3$ are alias terms for $\ddot{\theta}$ and $\ddot{\alpha}$, respectively. The state-space representation can be done by:

$$\begin{aligned} \dot{\mathbf{x}} &= \mathbf{A}\mathbf{x} + \mathbf{B}u \\ \mathbf{y} &= \mathbf{C}\mathbf{x} + \mathbf{D}u \end{aligned} \tag{6}$$

Where $\mathbf{y}$ is a vector containing the system output values (angular displacements θ and α, in that order). The system control vector is represented by u, in this application it is a scalar and a alias for V_m. The terms $\mathbf{A}$, $\mathbf{B}$, $\mathbf{C}$ and $\mathbf{D}$ represent state matrix, input matrix, output matrix and feed-forward matrix, respectively.

Table 1: System constant values used for modeling.

System property	**Value**
Pendulum mass (m_p), Kg	0.127
Pendulum length (L_p), m	0.337
Pendulum moment of inertia (J_p), $\mathrm{Kg}\cdot\mathrm{m}^2$	1.20×10^{-3}
Pendulum bearing shaft damping (B_p), $\mathrm{N}\cdot\mathrm{m}\cdot\mathrm{s}$	2.40×10^{-3}
Rotary arm length (L_r), m	0.216
Rotary arm moment of inertia (J_r), $\mathrm{Kg}\cdot\mathrm{m}^2$	9.99×10^{-4}
Rotary arm bearing shaft damping (B_p), $\mathrm{N}\cdot\mathrm{m}\cdot\mathrm{s}$	2.40×10^{-3}
Motor constant gain, (A_m), N·m / V	1.07
Motor damping, (B_m), $\mathrm{N}\cdot\mathrm{m}\cdot\mathrm{s}$	4.81
Gravity constant (g), $\mathrm{m/s}^2$	9.81

Substituting Eq. (3) into Eq. (2) and using the values for the system constants as listed in the Tab. 1, the state-space matrices are evaluated as follows:

$$\mathbf{A}=\begin{bmatrix}0 & 0 & 1 & 0\\ 0 & 0 & 0 & 1\\ 0 & 81.366 & -27.829 & -0.930\\ 0 & 121.892 & -26.755 & -1.394\end{bmatrix},\quad \mathbf{B}=\begin{bmatrix}0\\ 0\\ 51.764\\ 49.767\end{bmatrix},\quad \mathbf{C}=\begin{bmatrix}1 & 0 & 0 & 0\\ 0 & 1 & 0 & 0\end{bmatrix},\quad \mathbf{D}=\begin{bmatrix}0 & 0\end{bmatrix} \tag{7}$$

The designed poles to be placed are represented by $\mathbf{J}=\begin{bmatrix}-2.80+2.86j & -2.80-2.86j & -30 & -40\end{bmatrix}$. The first two poles are conjugate pairs with damping ratio $\zeta=0.7$ and natural frequency $\omega_n=4\ \mathrm{rad/s}$, the other two are selected to increase the system responsiveness. As pointed out by Ogata (2010), the gain matrix, $\mathbf{K}$, can be defined using Ackermann's formula, its given by:

$$\mathbf{K}=\begin{bmatrix}-8.49 & 45.45 & -4.10 & 5.20\end{bmatrix} \tag{8}$$

Finally, a time based variable reference, $\mathbf{x}_{ref}$, is defined:

$$\mathbf{x}_{ref}^{\mathrm{T}}=\begin{bmatrix}\frac{\pi}{6}\,\mathrm{sgn}\left[\sin\left(\frac{2\pi\,t}{3}\right)\right] & 0 & 0 & 0\end{bmatrix} \tag{9}$$

It can be interpreted as an input to the control system that modify the error periodically and forces the rotary arm to rotate from $-\pi/6\,\mathrm{rad}$ to $6/\pi\,\mathrm{rad}$ and vice-versa in a period of 3 seconds, the expected behavior of each measured state is simulated and presented in the Fig. 2.

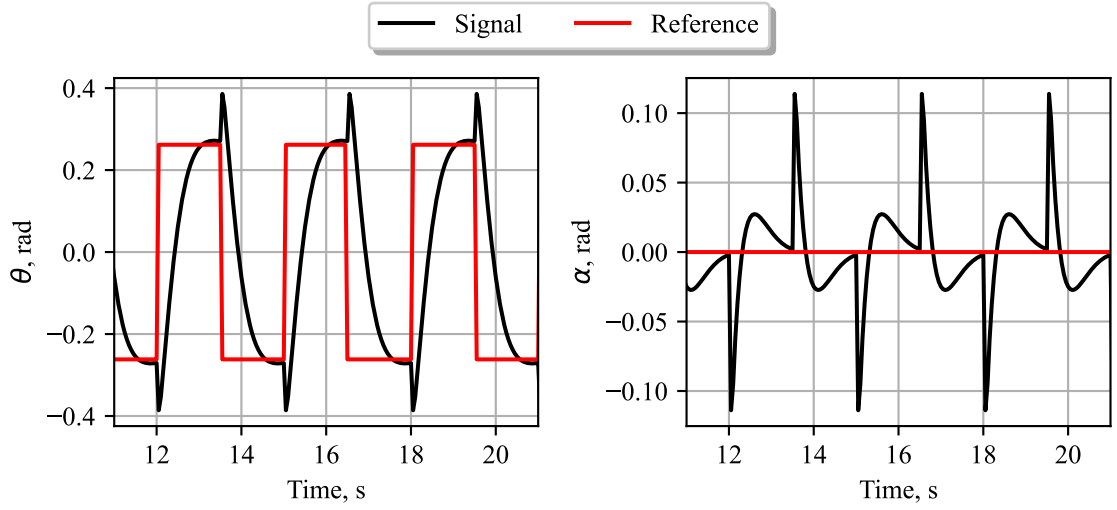

Figure 2: Linear controller with variable rotary arm reference simulation.

3. STRUCTURAL HEALTH MONITORING

The periodic monitoring of a structure serves the purpose of assessing its structural integrity, identifying existing stages of damage, and determining the feasibility of its continued use. Farrar and Worden (2007), Figueiredo *et al.* (2009) and Tokognon *et al.* (2017) outline four systematic steps for implementing a Structural Health Monitoring (SHM) system: operational evaluation, data acquisition and manipulation, feature extraction, and statistical modeling for feature classification. This section will detail these steps and comment on the results obtained.

3.1 Operational evaluation

The operational evaluation involves addressing specific inquiries related to the monitored system. In this study, the RIP was chosen as the reference system, with the key focus being the utilization of variables already monitored for the control system. By doing so, the developed SHM approach highlights how control variables can be employed for damage detection in systems that exhibit repetitive and predictable motion, without external perturbations. This enables the generation of evaluative metrics without incurring additional hardware costs.

3.2 Data acquisition and manipulation

The data acquisition step is straight forward in this process given the nature of the proposed approach, it consists of storing the controller state variables only for the collected variables, that is, the angular displacements, used for monitoring propose. Derivative data such as angular velocities are left behind as this process is carried out mathematically. To recreate the oscillatory behavior observed in the simulation, an experimental apparatus is constructed. Time series data are collected for each operating condition, beginning with the healthy (default) state and subsequently the damaged states.

(a) Mass fixed to the pendulum tip.

(b) Operation in CD condition.

Figure 3: Assembly and experimental execution.

The damage caused to the structure is non-destructive, it artificially adds CD and AD. The CD is simulated by adding masses to the pendulum tip, in one case 4.77 grams (small mass), in the second case 14.70 grams (large mass), while the AD type damage is induced by modifying the motor saturation via software, a reduction from ± 6 Volts to ± 3 Volts (saturation). Figures 3a and 3b show how the mass was fixed at the tip of the pendulum and an instant of its operation in CD condition, respectively.

The first step in data manipulation is to remove the initial and final transients from the raw signals, it is done by subtracting the initial and final 20 seconds. Then, they were divided into samples with two periods – 6 seconds – starting from the movement performed by the rotary arm, its position was taken as a reference for the selection of the indices that constitute each sample in both signals. The analysis indicates 326 passes through the origin, to satisfy the established time criterion it is necessary that the rotary arm passes through the origin four times, resulting in 81 different samples for each condition for each signal, each with approximately 3003 points. It's a total of 324 samples per signal.

The hardware used collects data with a sampling rate of 500 Hz, however, small fluctuations may occur, so this step

also treats this data, in order to make the time series of equal size. This was done by a generated function that returns a polynomial with the degree equal to the initial number of points in the sample and without smoothing between the points, that is, connected by a straight line, then a vector of 3003 equally spaced points was generated starting at 0 and ending at 6 seconds, this was replaced in the function, the return of this operation represented the new vector for the sample.

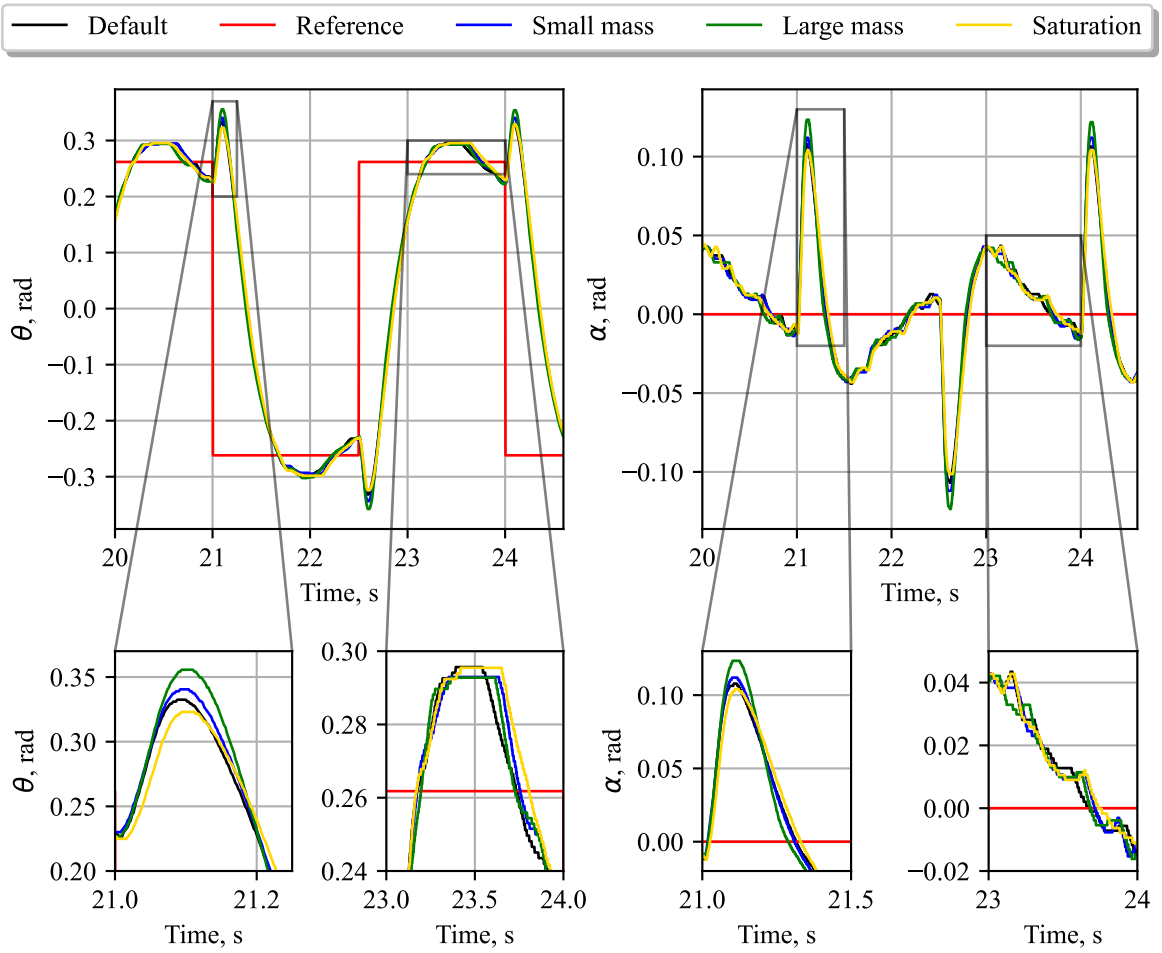

Figure 4: Sample data from collected signals, θ and α.

A sample of each collected signal, in each condition, is represented in Figure 4. The subplots present, in details, regions where it is possible to verify fluctuations in the values related to each condition.

It is noticeable in the zoom of the signals, for both sensors, that quantization effect occurs, firstly because the signal is digital, therefore it is discrete, in addition, the encoders used have 12-bits and work in the range of 0 to 2π, so the minimum value they can register is 0.0015 rad. As the application of this work focuses on a small set of sensors' workspace the quantization effect becomes more evident. This effect will be considered tolerable in the analysis, as it is still possible to notice that there is considerable differentiation between the curves of each signal, in addition, at points with greater amplitude variation, quantization is much less significant.

3.3 Feature extraction

Feature extraction will be done by the implementation of an AIS based on the classic view of NIS. This uses the NS to generate affinity indicators between a sample and a given reference group, this will be the feature used for damage detection and classification. The implemented concepts are seen in Forrest *et al.* (1994), Lima *et al.* (2013) and Almeida (2022). The algorithm conceptually replicates the biological functioning of the T cells NS. It is divided into two stages, Censoring and Monitoring. Figures 5a and 5b show the flowcharts with the commands executed by the algorithm in each phase.

The censoring step is when the algorithm "learns" which samples are self (to compose the baseline) from known default data, this is done by randomly selecting samples from a known set, in this paper two baselines were created for damage detection, one for each sensor. In the Monitoring step, with the baseline defined, a sample that will be monitored, goes through the equivalence checking process in relation to the entire set of self-detectors, if a minimum percentage of

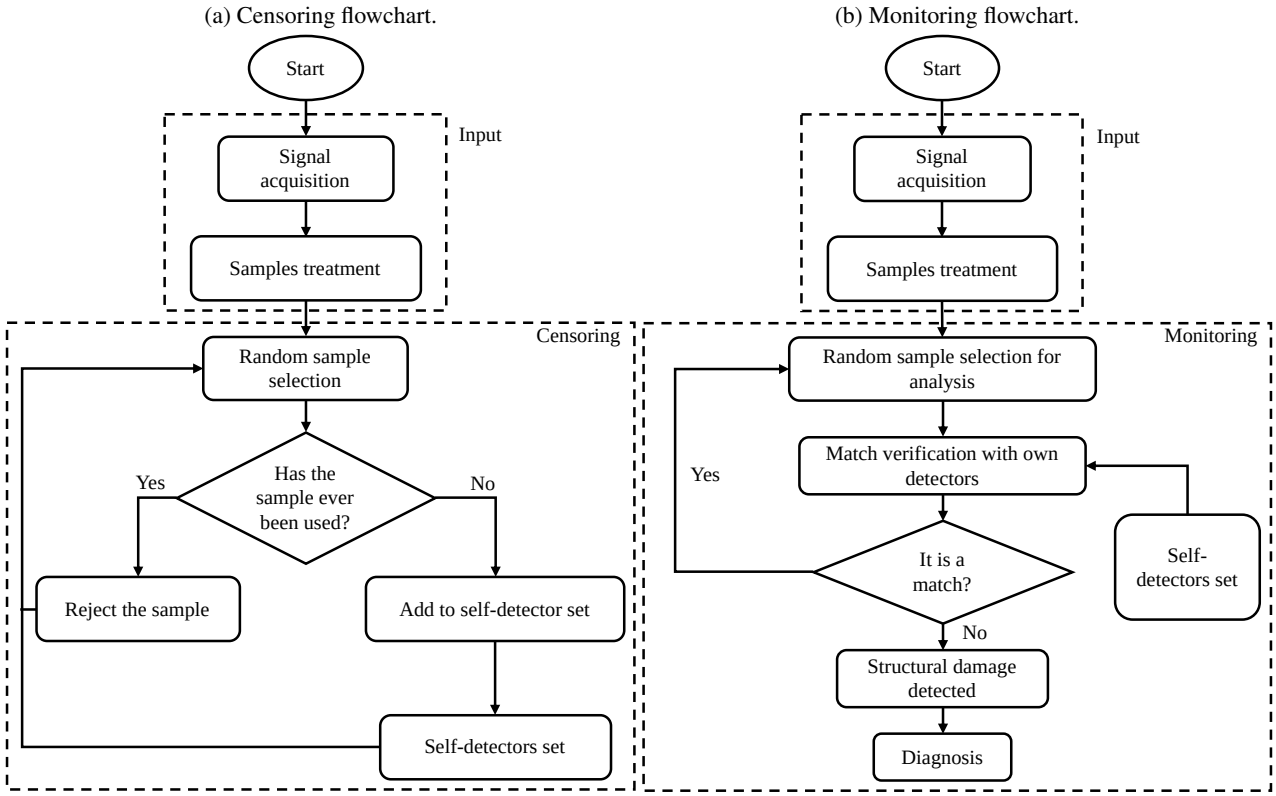

Figure 5: Negative Selection Algorithm flowcharts.

affinity is reached for at least one of the baseline samples, this one is called self, otherwise a non-self sample is detected. This process works analogously to mature T-cells, the detectors act as antibodies and the unknown signals as antigens. (Forrest *et al.*, 1993, 1994; Almeida, 2022)

Equivalence checking involves comparing a sample under analysis to a second sample, assessing compatibility point-by-point with upper and lower tolerance thresholds. For a point to be considered compatible, its value must fall within the tolerance range. To determine overall equivalence, a predetermined percentage of points must be classified as compatible. This method of point-by-point comparison, as outlined by Lima *et al.* (2013) and Almeida (2022), acknowledges the minimal probability of absolute point equality between samples and allows for a tolerated deviation by defining maximum and minimum variation limits of reference sample values. (Forrest *et al.*, 1994)

The percentage of points that are classified as compatible is defined as the affinity rate between the samples, and is given by:

$$\mathcal{T}_a = \frac{\mathcal{A}_n}{\mathcal{A}_t} \times 100 \tag{10}$$

Where $\mathcal{T}_a$ is the affinity rate between samples given in percentage, $\mathcal{A}_n$ is the number of points that fall within an acceptable tolerance range, and $\mathcal{A}_t$ is the total number of analyzed points.

The tolerance range is described mathematically as:

$$\underline{\mathcal{A}_b^i} \leq \mathcal{A}_g^i \leq \overline{\mathcal{A}_b^i} \tag{11}$$

Where $\mathcal{A}_g^i$ is the nominal value of element i in the reference sample, $\underline{\mathcal{A}_b^i}$ and $\overline{\mathcal{A}_b^i}$ are the nominal value minus and plus the adopted tolerance deviation in the i element, respectively. In these paper, these deviations are applied proportionally and symmetrically to the value of the element i.

The determination of the upper and lower intervals, $\underline{\mathcal{A}_b^i}$ and $\overline{\mathcal{A}_b^i}$, were set manually, as an example, Almeida (2022) used the value of $\pm 0.01\%$, while Lima *et al.* (2013) used $\pm 3\%$, in this work the values used were determined so that the detection rate was optimized, while the non-self signals remained distinct from each other for adverse conditions. For example, if this value is too small, the final affinity rate between the samples would be indistinguishable, on the other hand, if it is too large, samples under different conditions may generate equivalence results and disturb the classifier.

The definition of the minimum affinity rate, $\mathcal{A}_f$, must be handled on a case-by-case basis, and its variation must be analyzed, as done by Forrest *et al.* (1994). In some cases self signals may have high affinity with each other, while in other cases this affinity may be reduced. The determination of affinity rates, for each signal analyzed in this work, was done manually until an optimal point was found. The form of definition used measures the average affinity between the samples of the healthy dataset (default), this value is used as a starting point, then variations are performed until there is optimization of the results following the same principles used for the intervals.

According to Almeida (2022), it is pertinent that the baseline training samples rate do not compose a number greater than 70% of all healthy signals. Following all these indications, the values used in this work, for each signal analyzed, are represented in the Table 2. Thus, the developed NSA, combining data from both sensors, is able to detect damage correctly 99.07% of the time with a *F1-Score* of 0.9938.

Table 2: Values used in AIS for each position signal.

AIS Property	**Rotary arm** (θ)	**Pendulum** (α)
Baseline training samples rate $(\mathcal{X}_t)$, %	69.14	69.14
Minimum affinity rate $(\mathcal{A}_f)$, %	93.50	30.00
Upper and lower limit rate $(\pm\mathcal{A}_{bi})$, %	$\pm$ 3.10	$\pm$ 3.00

Figure 6 shows, for the rotary arm (θ) and pendulum (α) signal, the comparison between a random sample and a random default sample (which compose the baseline), the red areas of both charts illustrate the upper and lower tolerance range, $\pm\mathcal{A}_b^i$. The points where the blue curve is located inside the red area, equivalences between the samples are counted, so the affinity of the sample is relative to the proportion of this value in relation to the total number of points.

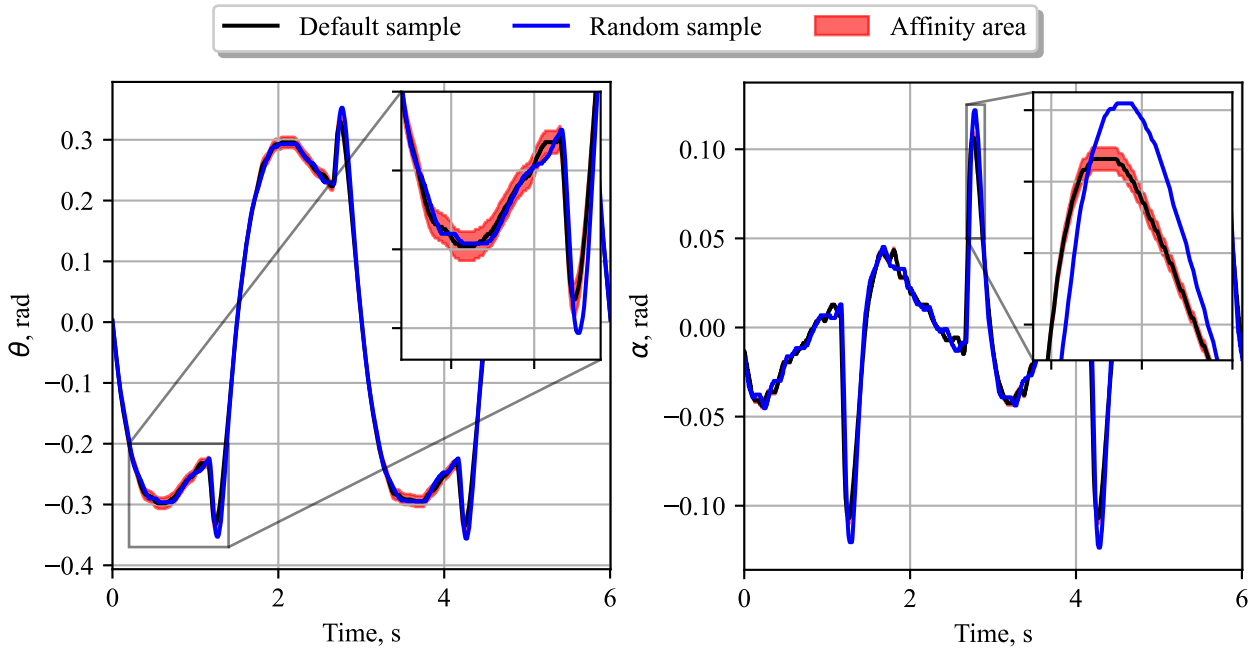

Figure 6: Linear controller with variable rotary arm reference simulation.

3.4 Statistical modeling for feature classification

The affinity of a sample in relation to the baseline is easily converted into the classification of its structural condition, in this case, whether it has damage or not, this is done just by comparing the result to the pre-established minimum affinity rate, $\mathcal{A}_f$.

This was the process performed to determine whether a pair of sibling samples made up the set of samples with or without damage, and whether this classification was done correctly. A pair of sibling samples means that both samples belong to the same moment in the data collection time series, in this case, when the AIS result is given, if any of the two samples indicate damage, the pair of samples returns damaged as a diagnosis, on the other hand, the healthy state is only true if both samples indicate greater affinity than the predefined one in relation to their respective baseline.

The AIS was run 20 times in a row for each signal and in each run the baseline sample set was randomly recreated, so the detectors themselves were varied, and the results became different. Finally, an average of the obtained values was

performed, which indicated the average global performance of the algorithm. Table 3 indicates the results obtained in the form of a confusion matrix.

Table 3: Average confusion matrix from 20 random baseline generations.

		Real condition	
		Damaged	**Healthy**
Predicted condition	**Damaged**	242	2
	Healthy	1	79

For the classification process, the dataset of known samples is modified. In this case, for each set of samples of each signal and condition, a unique baseline is generated, where 69.41% of the samples (or 56 samples) that make up this set are randomly selected. In this way, four baselines are formed per signal, a sample that will be classified goes through the calculation of average affinity in relation to each baseline, its classification is given by the highest affinity rate obtained. As the signal samples are composed of sibling pairs, the final result is given by the average affinity rate between both for each condition, the highest affinity to condition value being used as the result. Table 4 shows the classification results obtained with signal combination.

Table 4: Average classification results with combined signals from 20 random baseline generations.

	Combined signals			
Condition	**Real count**	**Correct test count**	**Incorrect count**	**Success rate, %**
Default	81	100	0	100.00
Small mass	81	100	0	100.00
Large mass	81	100	0	100.00
Saturation	81	100	0	100.00

3.5 Results discussion

The obtained results demonstrate the effectiveness of the utilized method in both damage detection and classification. The choice of employing an AIS with Negative Selection was motivated by the periodic and repetitive characteristics of the signals. It is observed that the affinity rate among the samples from the rotary arm is higher compared to the pendulum samples. This outcome is expected due to the actuated nature of the rotary arm, whereas the pendulum is indirectly controlled. Although this difference may suggest that the pendulum signal is less reliable, it is, in fact, advantageous as the affinity pattern observed in the rotary arm is also observed in the pendulum. By establishing a baseline, samples from various conditions are compared, generating thresholds that encompass each type of signal, with minimal confusion between them. The combination of both signals proves instrumental in mitigating classifier errors. Figure 7 illustrates the behavior described for each signal and its baseline.

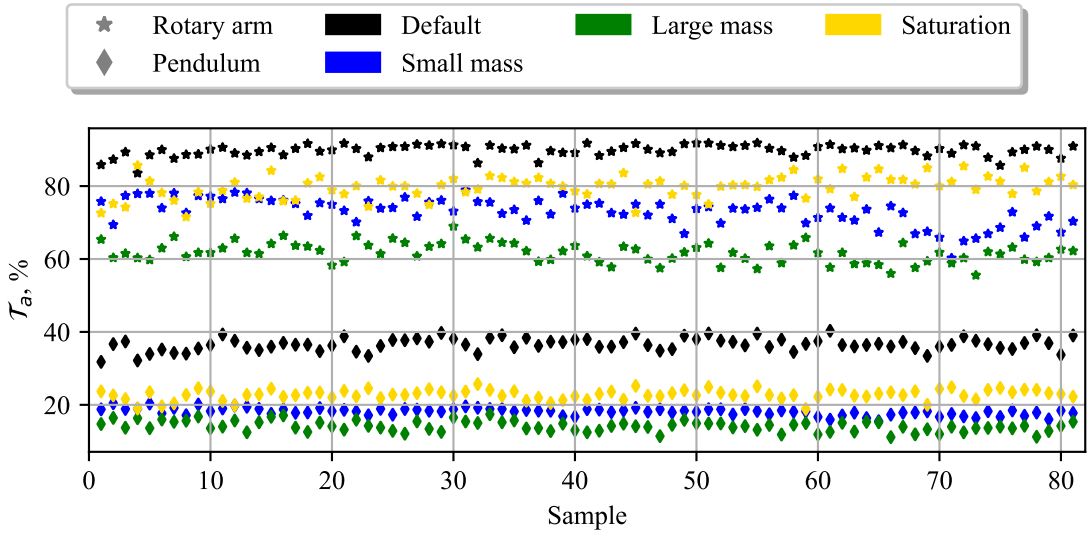

Figure 7: All samples' affinity from both signal in relation to each baseline.

4. CONCLUSIONS

The proposed method offers an approach for detecting damage in dynamic systems using a RIP as a reference model. This method can be implemented in dynamic systems that share the same characteristic, such as being periodic and repetitive for damage detection or classification of known operational states. A welcome side effect of this type of monitoring system is that it would also work to detect disturbances, as these would alter the expected affinity rates. As a data-driven process, there is naturally a need for data collection, however, once the baseline is formed, the damage detection process takes place quickly and proportionally to the period of system activity. This type of AIS based on NS proved to be efficient in detecting patterns in different types of real systems, the authors believe that its application should be carried out in other dynamic systems to expand this validation. Another point to increase the usefulness of this type of system is the generation of unsupervised classification methods, eliminating the need to generate baselines for unknown conditions.

5. ACKNOWLEDGEMENTS

We thank UNESP Ilha Solteira for providing the control laboratory and equipment used to run the tests. This work was funded by CAPES under grant number 88887.678338/2022-00.

6. REFERENCES

Almeida, E.F., Ferreira, L.V.G. and Chavarette, F.R., 2022. "Quantificação de dano em uma placa de material compósito com variação de temperatura utilizando sistema imunológico artificial". *XI CONGRESSO NACIONAL DE ENGENHARIA MECÂNICA*.

Almeida, E.F., 2022. *Sistema Imunológico Artificial aplicado no Reconhecimento de Falhas de uma Placa de Material Compósito*. Mestrado em engenharia mecânica, Universidade Estadual Paulista, Ilha Solteira, SP.

Dorf, R. and Bishop, R., 2017. *Modern Control Systems (thirteenth Edition)*. Pearson.

Engelbrecht, A.P., 2007. *Computational Intelligence: An Introduction: Second Edition*, John Wiley & Sons. Computational Intelligence: An Introduction: Second Edition.

Farrar, C.R. and Worden, K., 2007. "An introduction to structural health monitoring". *Philosophical Transactions of the Royal Society A: Mathematical, Physical and Engineering Sciences*, Vol. 365, No. 1851, pp. 303–315.

Farrar, C.R. and Worden, K., 2012. *Structural Health Monitoring: A Machine Learning Perspective*.

Figueiredo, E., Park, G., Figueiras, J., Farrar, C. and Worden, K., 2009. "Structural health monitoring algorithm comparisons using standard data sets".

Forrest, S., Allen, L., Perelson, A.S. and Cherukuri, R., 1994. "Self-nonself discrimination in a computer". In *Proceedings of the IEEE Computer Society Symposium on Research in Security and Privacy*. pp. 202–212.

Forrest, S., Javornik, B., Smith, R.E. and Perelson, A.S., 1993. "Using genetic algorithms to explore pattern recognition in the immune system". *Evolutionary Computation*, Vol. 1, No. 3, pp. 191–211. doi:10.1162/evco.1993.1.3.191.

Frank, P.M., 1990. "Fault diagnosis in dynamic systems using analytical and knowledge-based redundancy. a survey and some new results". *Automatica*, Vol. 26, No. 3, pp. 459–474.

Franklin, G., Powell, J. and Emami-Naeini, A., 2010. *Feedback Control of Dynamic Systems*. Pearson.

Isermann, R., 2006. *Fault-diagnosis systems: An introduction from fault detection to fault tolerance*, pp. 1–475. Fault-Diagnosis Systems: An Introduction from Fault Detection to Fault Tolerance.

Lima, F.P.A., Lotufo, A.D.P. and Minussi, C.R., 2013. "Artificial immune systems applied to voltage disturbance diagnosis in distribution electrical systems". In *2013 IEEE Grenoble Conference*. pp. 1–6. doi:10.1109/PTC.2013.6652127.

Machado, E.R.M.D., 2007. *MODELAGEM E CONTROLE DE SISTEMAS FUZZY TAKAGI-SUGENO*. Doutorado em engenharia elétrica, Universidade Estadual de São Paulo, Ilha solteira.

Ogata, K., 2010. *Modern Control Engineering*. Prentice Hall.

Rao, S., 2009. *Vibrações mecânicas*. Pearson Prentice Hall.

Sohn, H., 2007. "Effects of environmental and operational variability on structural health monitoring". *Philosophical Transactions of the Royal Society A: Mathematical, Physical and Engineering Sciences*, Vol. 365, pp. 539–560.

Talbi, E.., 2009. *Metaheuristics: From Design to Implementation*. Metaheuristics: From Design to Implementation.

Tokognon, A. C., J., Gao, B., Tian, G.Y. and Yan, Y., 2017. "Structural health monitoring framework based on internet of things: A survey". *IEEE Internet of Things Journal*, Vol. 4, No. 3, pp. 619–635.

Yang, J.., Shim, S.., Seo, J.. and Lee, Y.., 2009. "Swing-up control for an inverted pendulum with restricted cart rail length". *International Journal of Control, Automation and Systems*, Vol. 7, pp. 674–680.

7. RESPONSIBILITY NOTICE

The authors are solely responsible for the printed material included in this paper.